Analysis of Growth Mechanisms and Microstructure Evolution of Pb+2 Minor Concentrations by Electrodeposition Technique

Ahmed Rebey (ahmed.rebey@fsm.rnu.tn)
Qassim University College of Science https://orcid.org/0000-0002-7541-9573
R. Hamdi
Imam Abdulrahman Bin Faisal University
B. Hammami
Qassim University

Research Article

Keywords: Electrodeposition, Water purification, Toxic heavy metals, Pb II concentration, Growth mechanism

Posted Date: September 29th, 2021

DOI: https://doi.org/10.21203/rs.3.rs-940906/v1

Version of Record: A version of this preprint was published at The European Physical Journal Plus on March 1st, 2022. See the published version at https://doi.org/10.1140/epjp/s13360-022-02345-y.

Analysis of growth mechanisms and microstructure evolution of Pb^{+2} minor concentrations by electrodeposition technique

A. Rebey[1 *], R. Hamdi[2,3] and B. Hammami[4]

[1] *Department of Physics, College of Science, Qassim University, PO Box 6622, Buraidah, Qassim, Saudi Arabia*

[2]*Department of Physics, College of Science, Imam Abdulrahman Bin Faisal University, P.O. Box 1982, 31441, City of Dammam, Saudi Arabia.*

[3] *Basic and Applied Scientific Research Center, Imam Abdulrahman Bin Faisal University, P.O. Box 1982, 31441, Dammam, Saudi Arabia.*

[4]*Department of Chemistry, College of Science, Qassim University, PO Box 6622, Buraidah, Qassim, Saudi Arabia*

Abstract

In this study, the electrodeposition technique has been used to deposit low concentrations of highly toxic lead (Pb) cations into a solution of nitrate at a constant potential of -1V on fluorine-doped tin oxide electrodes (FTO). Monitoring of the reaction was conducted with the assistance of a computerized potentiostat/galvanostat setup, in cyclic voltammetry and *in situ* chronoamperometry modes. X-ray diffraction, scanning electron microscopy, energy dispersive X-Ray, and ultraviolet-visible spectroscopy techniques were used to examine the crystal structure, morphology, and optical properties of the lead deposits, respectively. Pb regular micro-

hexagons have been identified; their size and density were significantly influenced by the cationic precursor's concentration. The correlation between the morphological and crystallographical structures of the electrodeposits was discussed. Based on chronoamperometric measurements, a mechanism for the growth of Pb deposits on FTO substrate has been proposed. Based on the reported results, electrodeposition processes of low heavy metals concentrations in contaminated water could be optimized using the eco-friendly electrodeposition technique.

Keywords: Electrodeposition; Water purification; Toxic heavy metals; Pb II concentration; Growth mechanism.

*Corresponding author: ahmed.rebey@fsm.rnu.tn (Pr. Ahmed Rebey).

1. Introduction

Since heavy metals (HM) such as arsenic (As), tin (Sn), antimony (Sb), copper (Cu), and lead (Pb) are not biodegradable, their toxicity depends mainly on how much bioaccumulation occurs in the living system. As a result, heavy metal contamination of water sources has been causing concern recently.

Lead is one of the most hazardous HM pollutants since it adheres easily to soft tissues and bones. Additionally, it causes severe damage to ecosystems; for example, it causes complex physiological, genetic, and biochemical changes in plants. Pb leaks into the living system cell mainly through the water. In this regard, the World Health Organization (WHO) and the Food and Agriculture Organization (FAO) of the United Nations have verified that the form of lead found in waste/drinking water is an important factor in general poisoning, according to their annual reports for 2011[1]. The sources of lead leakage to the water are multiple. For instance, Pb is abundantly used in the production of batteries, paints, and household appliances. It is, also, used as a solder in the food processing industry. The organo-lead compounds such as tetraethyl and tetramethyl lead are used extensively as antiknock and lubricating agents in petrol [2]. Additionally, because of Pb dissolution from natural sources and residual chlorine present in drinking water, Pb could also be found in tap water.

Due to varying concentration rates of lead in water, the toxicity level in the human blood varies from country to country and depends on the country's industrial orientation and living

style. So, a particular interest is given to optimizing remediation technologies used for water purification. Researchers found that using different synergistic techniques can improve the efficiency and functionality of industrial wastewater purification treatments. In this regard, we can mention the activated carbon (AC) which is one of the most used adsorbents to remove soluble compounds from water [3]. However, the AC process presents several disadvantages, among which are the high cost and the difficulty to be separated from the aquatic system after purification. The precipitation of metals as insoluble metal hydroxides obtained by increasing the pH of the solution is also a widely applied process [4]. However, this consumes and produces many chemicals difficult to get ridof. Biochemical and biological technologies are also emerging in this field [5]. Nevertheless, the use of this technology poses a wide range of challenges.

The electrodeposition (ED) technique is an attractive technology that proved its efficiency in removing HM frommetal-contaminated industrial wastewaterand showed an excellent elimination capacity, especially for high pollutant concentrations. It is *i*) simple, non-expensive, can be implemented under ambient conditions, and easily scalable to the industrial level. *ii*) It presents a high deposition rate and allows accurate control of the growing nanostructure properties (dimension and/or morphology) by adjusting the electrical parameters. *iii*) The obtained deposits are relatively compact, easy to be synthesized on template-based structures, and could be used for other industrial purposes. Therefore, a good knowledge of the parameters

involved during the electrodeposition process is required to achieve precise control of the properties of the removed clusters.

The ED has been used to remove lead from different chemical baths among them, the sodium nitrate solution, considered as the most preferred system to deposit lead clusters onto different types of electrodes such as graphite [6], indium-tin-oxide (ITO) [7], platinum [8], silver [9], and lead foils [10. However, it is believed that one of the greatest challenges is to capture lead from baths containing small cationic precursor concentrations.

In this work, we study the deposition of lead via the ED technique onto fluorine-doped tin oxide (FTO) electrode in a $NaNO_3$ solution. The experiments are performed for low concentrations of Pb II. The measurements are done either in cyclic voltammetry (CV) mode or *in situ* chronoamperometry mode. The deposits of lead were characterized by energy dispersive X-Ray (EDX), ultraviolet-visible (UV-VIS) spectroscopy, X-ray diffraction (XRD), and scanning electron microscopy (SEM) instruments.

2. Experimental

2.1 Chemicals and materials

Using double-distilled water, sodium nitrate ($NaNO_3$, 99.99%) was dissolved until it formed a homogeneous, transparent, colorless liquid. lead II nitrate ($Pb(NO_3)_2 \geq 99.0$ %) was used as a

cationic precursor (Pb^{2+}). FTO conductor glass with resistance 13 ± 0.2 Ω/ square and thickness of 2.2 mm was used as substrate.

As known, by modifying the electrode structure, the nucleation energy, size, and shape of the electroplated deposits can be modified. In this regard, the use of FTO substrates for metal electrodeposition has long been considered among the top options[11]. Probably, because they offer an inert surface where it is possible to study nucleation and growth process neglecting the metal-metal interaction. Another reason to encourage the use of these substrates is that it has become possible to manufacture them by a low cost-effective and environmentally friendly method (no fluorine gas is used, and no toxic effluent is produced) [12]. To guarantee the existence of extended terraces, the FTO substrates were rinsed with detergent, deionized water, acetone, and isopropyl alcohol before each experiment. Each rinsing step was carried out in an ultrasonic bath for 15 min, followed by drying at 80 °C.

2.2 Electrodeposition and characterization techniques

Electrochemical experiments are performed in a conventional three-electrode workingstation. The FTO substrate is used as the working electrode and a platinum wire (0.05 cm in diameter) is used as the counter electrode. For the reference electrode, we use an Ag/AgCl electrode in contact with the solution through a Luggin capillary. All the electrodes in the electrochemical cell were polished with emery paper, degreased with an anhydrous alcohol solution in an ultrasonic bath, and

cleaned with doubly deionized water before use. The voltammetry and *in situ* amperometry measurements were carried out at room temperature using a potentiostat/galvanostat setup. The minimum intensity which can be resolved by the potentiostat is 1 nA.

The structure and phase identification of the removed Pb electrodepositsare studied by X-ray diffraction, with CuKα radiation of 1.540 Å. The diffracted data are collected over the range $2\theta = 20° - 80°$ with a scanning step width of $0.02°$. The SEM imaging analyses were performed by a microscope equipped with energy-dispersive X-ray spectroscopy, EDX. The optical absorption was measured for the different samples at room temperature by using a UV–VIS spectrophotometer in the energy range $3.5 - 1.5$ eV.

2.3 Preparation of solutions

Samples labeled a, b, c, d, e, and f are the result of electrodeposition of lead by ED technique from solutions with different Pb^{2+} concentrations at equal time intervals (5000 s). A 0.4 Msolution of sodium nitrate (electrolyte solution) and Pb $(NO_3)_2$ were mixed in a molar ratio of 2 : 1. During each measurement, solutions of pH 5.4 are continuously stirred to ensure that chemical components have fully dissolved. The analytical grade chemicals were used to prepare the solutions as listed in Table 1.

Table 1. Solutions and chemical additives used to prepare the studied samples.

Sample	The concentration of lead II nitrate in the solution
a	4×10^{-3} M
b	6×10^{-3} M
c	10×10^{-3} M
d	12×10^{-3} M
e	16×10^{-3} M
f	20×10^{-3} M

3. Results and discussion

3.1. Cyclic voltammetry study

The ED experiments were carried out at the scan rate of 60 mV/s. Recorded cyclic voltammograms (I-V) represent the static diagram of current I versus voltage V at different concentrations of Pb^{2+} as shown in Table 1, and different temperatures in the interval of voltage [-1.5V and +1.5 V]; Figure 1 shows a comparison of the experimental I-V cycles obtained from the solutions with and without Pb^{2+} (reference cycle). These typical cyclic voltammograms show the variation in current peaks as a function of temperature from an aqueous solution of 4 mM Pb(NO3)2 in 0.4 M $NaNO_3$ (Figure1.a), and as a function of Pb^{2+} concentration @25°C from a solutions of 4 mM $Pb(NO3)_2$ in 0.4 M $NaNO_3$ (sample a), and 20 mM $Pb(NO3)_2$ in 0.4 M NaNO3 (sample f) (Figure 1.b). The presence of these peaks is associated with the presence of electrochemical processes on the electrode surface.

As shown in Figure 1.b, temperature changes can affect the peak intensity and position. In fact, by modulating bath parameters such as the applied potential (magnitude and type - DC or pulse), pH, and temperature, the electronic properties such as carrier concentration can be modified. Maintaining a constant temperature will ensure homogeneous dissolution across the total anode area during the anodization process. Abhijit Ray [13], however, reported that high temperatures speed up the chemical dissolution process. Consequently, working temperatures should usually be kept fairly low(~ambiant) so that the oxide does not dissolve completely. Choosing the bath temperature will obviously depend on the type of electrolyte and electrodes used. In order to achieve the desired results for our ED measurements, we fixed the bath temperature at 25°C for the rest of the study.

Figure 1b shows a good example of the chemical reduction of lead at the given temperature through the cycles shown (two typical cycles recorded for samples a and f are shown here for clarity). The presence of Pb cations in the baths led to the appearance of cathodic currents during the deposition of metallic lead (starting at about - 0.6 V). Due to the higher overpotential with lead, the background currents did not occur. In the absence of lead, the reference cycle I-V has a symmetrical shape and shows no current spike. In contrast, in the anodic scan of cyclic voltammetry I-V, a clear stripping peak of lead ionization around the potential -1 V is observed for all samples studied, although the amount of Pb II in the solutions is considered relatively low. This peak allows the regeneration of the electrode surface, its

voltagedoes not change with concentration, but its intensity has increased. The peak intensity varies proportionally with the concentration of Pb II; it reaches about 10 mA at -1V for sample a (4 mM $Pb(NO_3)_2$) and 15 mA when the concentration is 20 mM $Pb(NO_3)_2$ (sample f). The ionization processes are illustrated by the stability of the observed currents during repeated potential cycles (each scan is repeated for three consecutive cycles).

In general, the ionization of the cation species presents in the solution with two positive charges, Pb^{2+} to produce a neutral metal atom Pb on the cathode as a substrate is represented by,

$$Pb^{2+} + \quad 2\,e^{-}[solution] \quad \rightarrow \quad Pb\,(s)[FTO\ electrodes] \qquad (1)$$

In the above reaction, the charges are supplied by an external current source and the Pb cations are taken up to form solid deposits on the conductive substrate in the given time. The electroplating of these deposits consists of the reduction of the metal ions. The reduction of Pb ions generally leads to a positive charge in the solution, resulting in a neutral lead atom on the cathode. As will be shown later, the higher the concentration of Pb ions, the greater the number of adatoms removed and the more they eventually form a lattice [13].

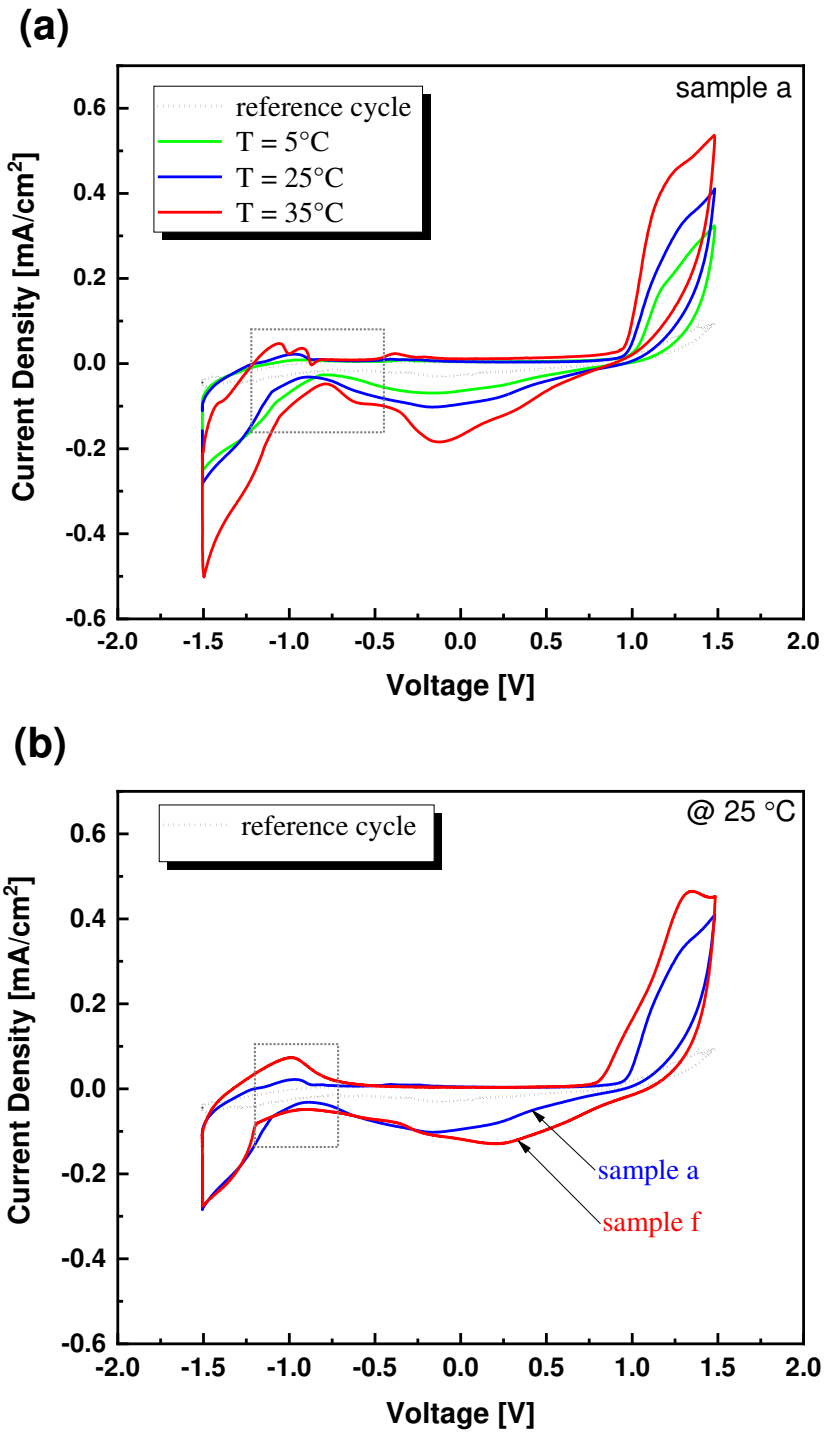

Fig.1. Typical cyclic voltammograms I-V measured for the FTO electrodes over the same voltage range [-1.5V and +1.5 V] showing the variation in current peaks (a) as a function of temperature from an aqueous solution of 4 mM Pb(NO3)2 in 0.4 M $NaNO_3$, and (b) as a function of Pb^{2+} concentration @25°C from a solutions of 4 mM $Pb(NO_3)_2$ in 0.4 M $NaNO_3$ (sample a), and 20 mM $Pb(NO_3)_2$ in 0.4 M $NaNO_3$ (sample f). The scan speed is 60 mV/s.

3.2 Electrodeposition process: Analysis of growth mechanism

To shed light on the removal process of lead by electroplating, the current density j is recorded as a function of time t in response to the applied potential pulse preconditioned in the region of complete lead ionization (-1V) (Figure2). The *in situ* evolution of the current transition shape shows a transition in the nucleation rate with increasing lead concentration II in the solutions. As reported by González-García and co-workers [14-16], the ED of lead is a very complex process that is strongly influenced by experimental conditions. Usually, the main factors that lead to the failure of this process are the low cation concentration or/and very low pH [17]. As a result, the experimental conditions chosen for the current study prove to be effective. It can also be concluded that the time factor is very influential, since the deposition process takes place in the nucleation control zone, despite the low levels of $Pb(NO3)_2$ in the solutions.

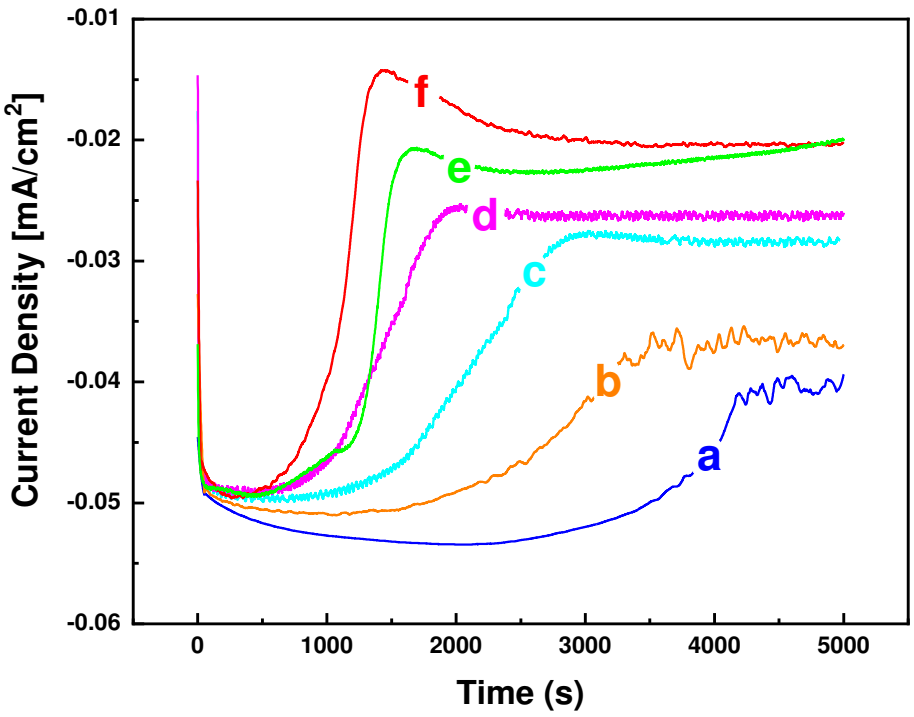

Fig.2. *In situ* measurements of current density transients *j* plotted against time *t* (chronoamperograms) @ 25°C. The electrical process was recorded in chemical baths with increasing amounts of lead ions: 4, 6, 10, 12, 16, and 20 mM led to the formation of samples a, b, c, d, e, and f, respectively.

The obtained chronoamperograms show very well-defined plateau effluxes defined by "S-shaped curves" [14]. As shown in Figure 2, these curves are typically characterized by three different phases describing the whole process. (*i*) First, the "silent phase", characterized by a sharp drop in the absolute current density followed by a relatively stable intensity. As can be seen in Figure 3.a, the duration of the silent phase ($\Delta t_{Ph\,1}$) decreases with the increase of lead ions. This means that the removal process strongly depends on the lead II nitrate concentration in the solution. (*ii*) The second phase, which begins when the current increases. The more the number of lead ions in the aqueous solutions increases, the faster the current density reaches its maximum value. This

can be seen quantitatively in Figure 3.b, where we show the evolution of the slope values ($S_{Ph\,2}$), as a function of the lead concentrations. Indeed, when the Pb II increases, $S_{Ph\,2}$ shifts to higher values, illustrating the concentration-dependent kinetics of Pb deposition on FTO substrates. (*iii*) Finally, the post-deposition phase, characterized by the stability of the currents. We can observe that during this last phase, the concentration of Pb deposits on the FTO surface reaches its equilibrium value and further accumulation of lead species is completely compensated by their release into solution. As suggested by Shtepliuket et al. [18], the accumulation limit depends on the concentration of reactive sites on the FTO surface. In other words, the strong control of the nucleation rate can be achieved by controlling the defect ratios in the epitaxial substrates, which are considered active detectors for heavy metals. Indeed, the deposition rates are proportional to the concentration of active lead ions in the solution. Depending on the electrical decomposition and the solution parameters, the nucleation of the lead deposits can be adjusted from one to two or three dimensions [19]. This could be discussed in light of structural and microstructural analysis.

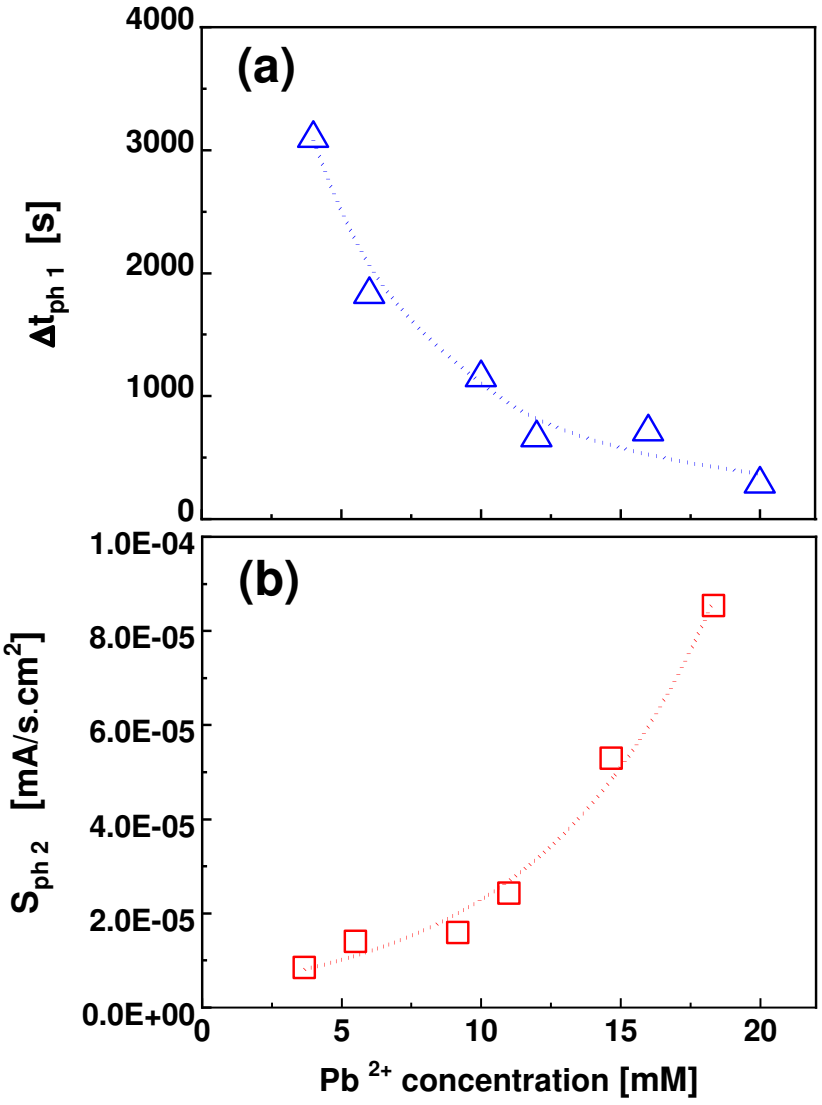

Fig.3. (a)The silent phase duration (Δt_{ph1}) as a function of Pb^{2+} concentration. (b) The evolution of the slope $S_{ph\,2}$ as a function of the concentration of lead ions in the solutions. The dotted curves in the insets are fitting curves.

3.3 Characterizationof samples

3.3.1. Optical characterizations

First, we perform UV-VIS absorption spectra of the different samples and the FTO glass substrate measurements under normal light incidence; the results show a clear influence of the concentration of the lead deposits on the light absorption properties. This could be due to the surface chemical and structural properties such as the degree of roughness, morphology, and stoichiometryof the Pb metal deposited on the FTO electrodes. Figure 4 shows the absorption spectra as a function of the energy in the range of 1.5 - 4 eV. Comparing the optical properties of the Pb deposits on the different glass substrates, it is clear that the electrodeposition process significantly improves the absorption of the stack.

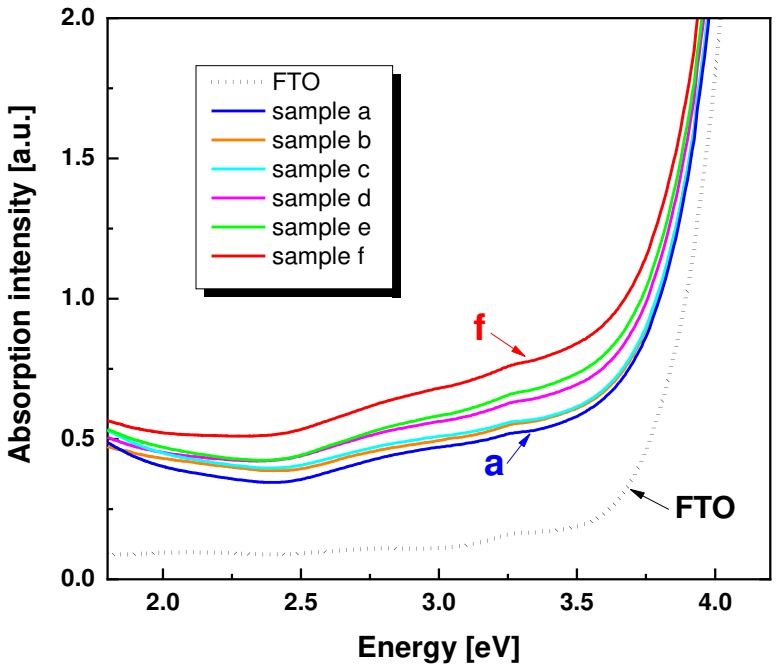

Fig. 4.UV-VIS absorption spectra of the samples a, b, c, d, e, and f; the control spectrum of FTO glass is also shown.

The absorbance of the samples decreases when they reach the range VIS. The decrease is more pronounced for FTO. Sample F shows the highest absorption intensity, which is probably due to a high coverage rate of Pb in sample F compared to the other samples. The absorption increases with the lead II concentration in the baths. In this case, sample f may be composed of microcrystallites of increasing density that result in a higher density of free charge carriers. In contrast, the FTO glass does not show free carrier absorption within the scanned energy range due to the low concentration of free carriers. Interestingly, a broad absorption peak is observed in all samples except FTO, spanning the energy range from 2.7 to 2 eV.In this case, one could interpret this behaviorthrough the use oflead's optical constants. Indeed, the formula $\alpha_{Pb} = \frac{4\pi}{\lambda} k_{Pb}$relates to the absorption coefficient of lead (α_{Pb}) to its extinction coefficient, k_{Pb}[20,21]. λ is the wavelength. Therefore, the change in absorption intensity is mainly due to the behavior of k_{Pb}. In this regard, Werner et al. [22] found that the real refractive index of pure Pb, n_{Pb}, exhibits a slow change as a function of λ, while the extinction coefficient at about2.4 eV shows important features, from which it can be concluded that the lead was deposited on the FTO glass substrates in good quality.

3.3.1 Energy dispersive x-ray analysis

As known, the crystalline structure determines the efficiency of the capture process and provides information on the associated growth mechanism. For this reason, we perform phase

identification and structural characterization by XRD SEM and EDXquantitative analysis of the electrodes before and after trapping the small amounts of lead.

As an example, we examine the surface quantitative analysis of sample C using energy dispersive x-ray analysis, Figure 5. Accordingly, Lead (Pb), Oxygen (O), Silica (Si), and Tin (Sn) are detected. From the inset, Pb occupies 23.52% of the 3D pie chart, O occupies 20.58%, Si occupies 2.35%, and Sn occupies 53.54%.As shown in sample c, Sn is the major component because it is the primary element of the Florine (F) doped SnO_2. F may be missed because of its low doping percentage. Si is present with a low percentage as it is covered by the FTO substrate. The presence of Pb is the result of the success of the electrodeposition process.

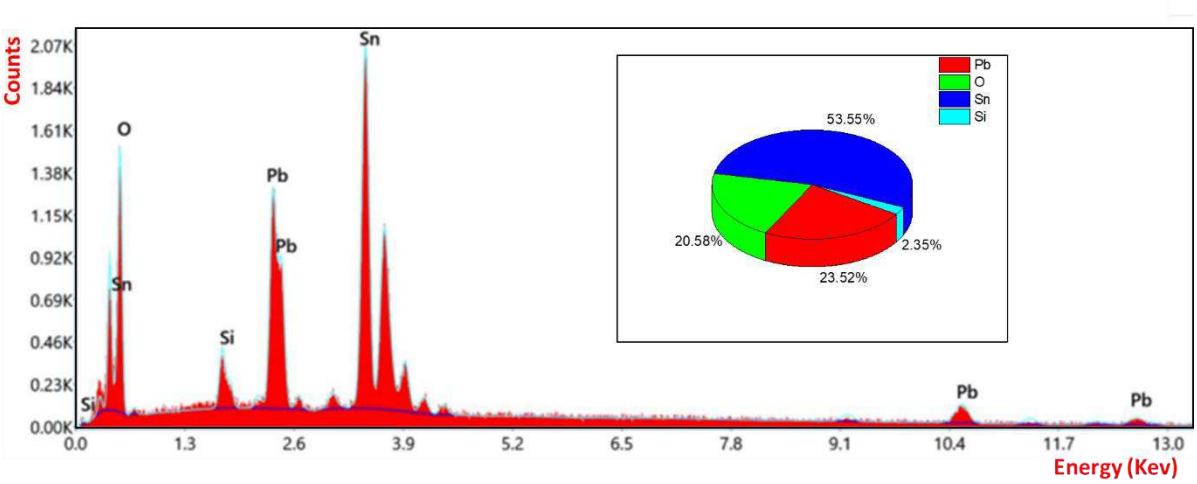

Fig 5. Energy-dispersive X-ray analysis (EDX) spectrum of lead deposit on FTO substrate at 25°C (sample c).

3.3.2 X-ray diffraction analysis

Figure 6 shows typical XRD patterns of the blank FTO and samples a, b, c, d, e, and f. The diffraction data were measured over the angular range 2θ= 20° - 80° with a scanning step size of 0.02°. As shown, all peaks on the diffraction pattern are sharp and correspond to Pb and the FTO substrate. The XRD pattern of the FTO issimilar to that of the standard pattern of SnO_2 in the cubic phase. The low crystallinity of the Pb crystals in the sample a is due to the low concentration of the corresponding active lead ions. However, a significant deposition of Pb on the FTO substrate can be observed in the remaining samples. The standard XRD peaks for Pb occur at angles of 2θ = 31.33°,36.35°,52.33°,62.28°,65.37° and 77.16°. A perfect overlap of the measured peaks with those reported in the literature by Yang and Reddy [23] and Pavlov [24]. As shown, the peaks of lead oxide are not found in the XRD scans. The obtained results confirm that Pb (II) cations were electrochemically reduced to Pb at -1 V. It is important to note that lead crystallizes in a face-centered cubic (FCC) lattice [25,26]. The planes of the growth layers are the most densely packed atomic planes of the crystal lattice. At this potential, a strongly preferential alignment in the (111) plane was observed in all electrodeposited films [27]. Therefore, the fraction of crystallites oriented in the other planes (100) and (110) is negligible. An examination of the XRD diffractograms in the *2θ* range of 35°-40° shows that the peak intensities at the 36,35°position generally increase with increasing lead addition in the solution (see inset of Figure 6). The difference in intensity is sufficient evidence for the existence of a

highly crystalline phase [28]. This indicates that the crystallinity of the composites is increased. Based on the obtained patterns, we conjecture that samples e and f have more regular and better-oriented crystals compared to the rest of the samples. To verify this conjecture, the morphological characterization of the deposited lead should be discussed.

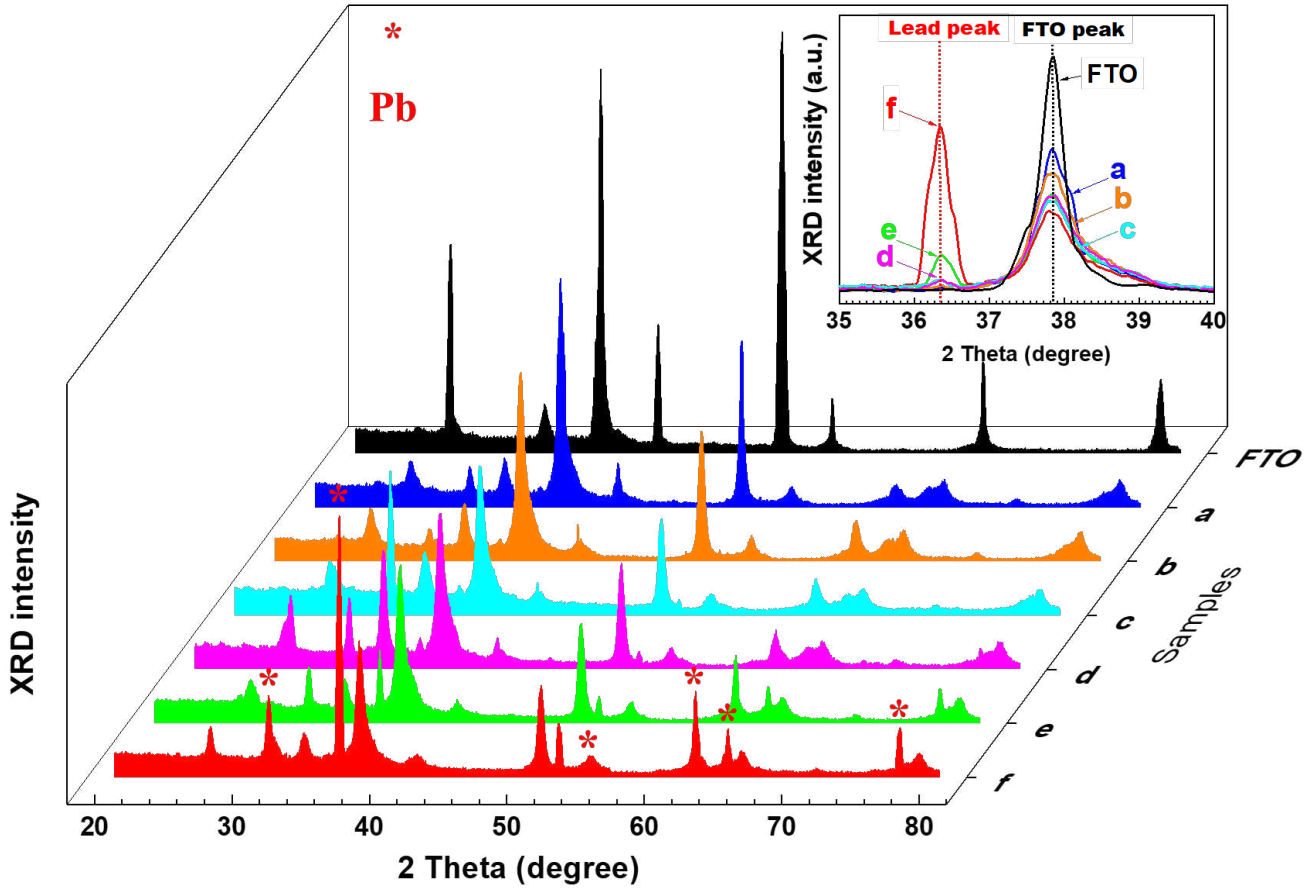

Fig. 6. (a) XRD patterns of the blank FTO and the other samples studied (A, B, C, D, E, and F). (b) Characteristic peak positions of FTO and lead in the 2θ range 35°- 40°.

3.3.3 Scanning electron microscopy

The electrodeposition process could allow the mass synthesis of lead. We believe that a good understanding of the growth kinetics and detailed knowledge of the deposit morphology is required to achieve precise control of the studied process. Figure 7 shows the observation of the evolution of the microstructure of the Pb deposits in samples a, b, c, d, e, and f using a scanning electron microscope: the surface of sample A shows lead deposits coalescing into small spherical nano-crystallites. The other samples show micro-hexagons with apartment faces and sharp edges and corners that have an angle of 120°. These hexagonal crystal plates "under construction" correspond to the 3D growth mode. Both their density and size change significantly. This proves that the nucleation mode strongly depends on the concentration of the cationic precursor, which allows correlating the morphology of metal deposits with their chronoamperograms.

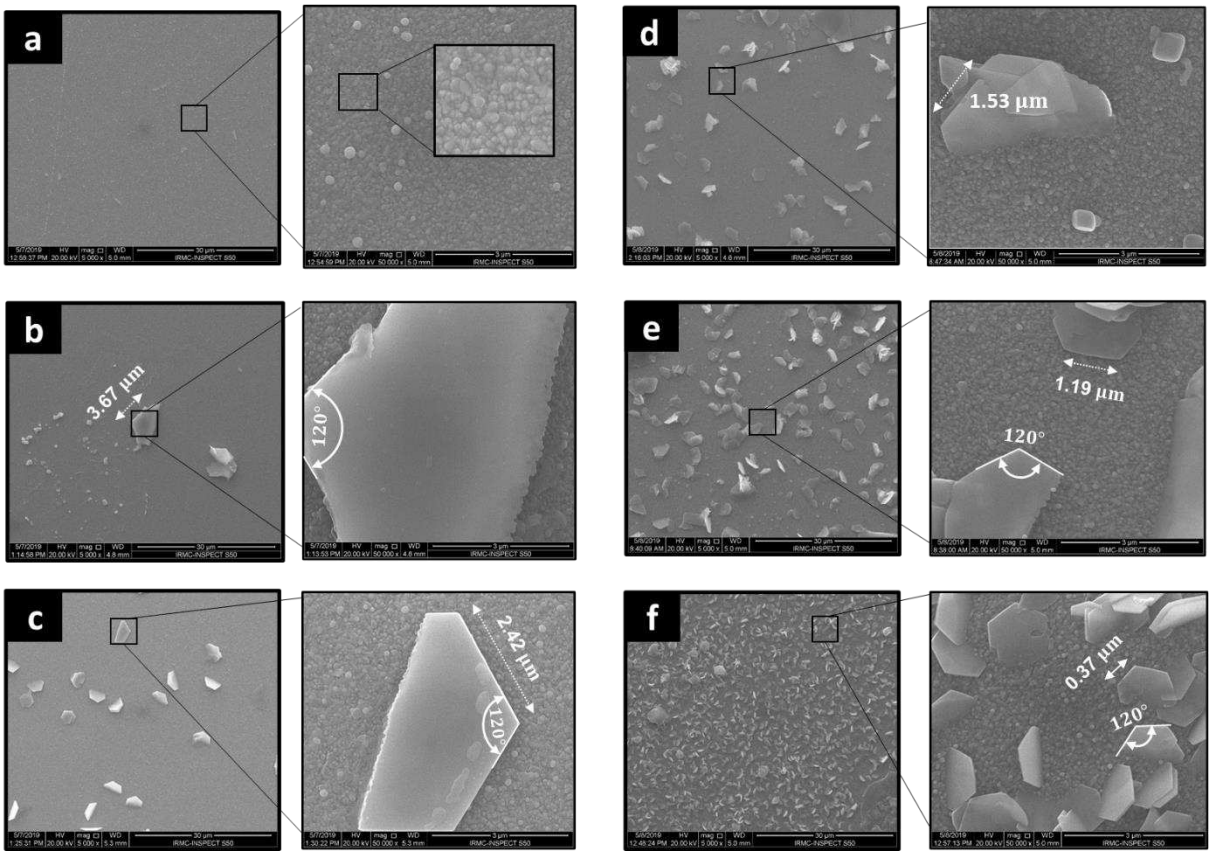

Fig.7. SEM micrographs of Pb deposits on FTO electrodes synthesized by ED in solutions of different Pb (II) concentrations, a: 4 mM $Pb(NO_3)_2$, b: 6 mM $Pb(NO_3)_2$, c: 10 mM $Pb(NO_3)_2$, d: 12 mM $Pb(NO_3)_2$, e: 16 mM $Pb(NO_3)_2$, and f: 20 mM $Pb(NO_3)_2$.

According to Stojan Djokić[29], the shape of the accumulated crystals is attributed to electrodeposition, either under ohmic control (OC) or under diffusion control (DC). Depending on the bath parameters affecting the core of the deposition process, such as the concentration of individual ionic species, the composition of the electrolyte, the temperature and the applied potential, various lead deposits, e.g., dendritic [30], needle-like [31], fern-like dendrites [25] and honeycomb-like structures [32], could be obtained.

The hexagonal regular crystal structure is the typical depositional morphology formed under the ohmic control zone [29]. The obtained morphologies are consistent with the analytical results of the Cottrell equation [33], which mathematically establishes a linear correlation between the properties of the deposits and the deposition rate. It is noticeable that the size of the hexagons is larger at lower concentrations of cations in the baths and gradually decreases with increasing concentration. The ridge size of these hexagons decreases approximately to one-tenth from sample b (6 mM $Pb(NO_3)_2$) to sample f (20 mM $Pb(NO_3)_2$). In sample f, a sand-rose-like morphology is observed, resulting from the fusion of a large group of regular hexagonal crystals of the same size. As the concentration of cations in the baths increases, so does the density of the deposits. Samples e and f contain more regular microcrystallites with better-oriented crystals compared to the other samples. This fact is in excellent agreement with the XRD diffractograms obtained. The regular crystals arise only from these hexagonal crystal faces and therefore represent single crystals with (111) orientation. Similar results have been reported by Rajamani et al [34] and Gupta et al [35]when performing the electrodeposition of bismuth on copper and ITO electrodes respectively.

Due to the large number of atoms involved and the constantly changing surface properties, the description of the nucleation process of lead atoms as a function of time appears to be very complicated. However, by combining the crystallographic and microstructural results with those

obtained from *in situ* chronoamperometry measurements, we propose the following scenario, Figure8, to describe the process of electrodeposition of lead II -minor concentrations:

I. Initially, the absolute current follows an initial sharp drop due to the induction time. According to Zimmer et al.[36] and Paunovic et al.[37], this chronoamperometric transient behavior is characteristic of diffusion-limited growth. Then, the deposition of lead atoms on the FTO surface occurs by electron transfer.

II. During the silent phase, the deposited Pb atoms diffuse over the substrate surface. These developments can be correlated with the growth of an ultrathin effective layer of diffused adatoms, leading to the formation of a high density of fine lead grains, as shown in Sample A. Accordingly, the effective layers flow out from these centers and fuse incompletely due to the active diffusion of lead atoms. In sample A, we observed the longest silent phase, which is synonymous with an important surface diffusion process taking place during this phase. This is in good agreement with the results reported by Katayama et al. [38] in BMPTFSA ionic liquid containing Pb $(TFSA)_2$ and Liu et al. [39] in PbO–urea-BMIC.

III. The formation and growth of 3D micro-hexagons rise when the absolute current transient starts to increase. Then, the growth of the hexagonal crystallites is observed according to progressive nucleation under a linear growth rate. The less the chronoamperogram's slope, the smaller the density of the dendrites. This may suggest that high cationic concentrations accelerate the growth rate, which in turn activates more nucleation centers. As we mentioned

before, some of the observed hexagonal crystallites are ‘‘under construction’’, is this way we suggest that when the 3D clusters begin to form, their growth flows slowly and often stops before they have reached the entire hexagonal shape. In that time, new ones are formed before the forerunners have reached their final size so that at certain times a great many incomplete micro-crystallites exist simultaneously.

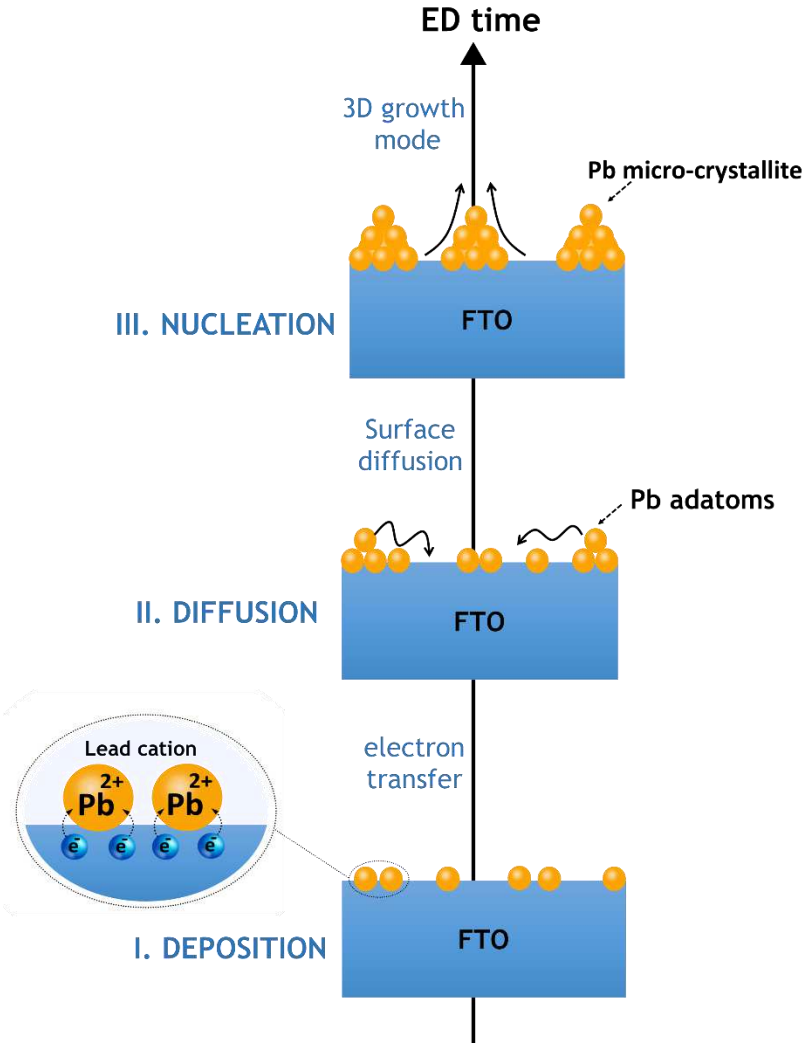

Fig.8.Illustration of the growth mechanism proposed to describe the electrodeposition of minor concentrations of lead II.

4. Conclusion

We have investigated the electrodeposition of toxic lead at a low concentration from a nitrate bath (0.4 M $NaNO_3$) at a constant potential of -1 V on FTO electrodes using CED. Chronoamperograms measured *in situ* showed a relevant transition of the growth mechanism and nucleation rate. This fact was underlined by the strong influence of cationic concentration on the recorded current density transients. The XRD measurements confirmed that the process of electrodeposition of lead was successfully carried out. As a result, hexagonal deposits of different sizes and densities are obtained by adjusting the lead concentration in the solutions. The correlation between the morphology and the crystallographic structures was discussed by considering the different nucleation modes. The absorption in the UV-VIS region of the different electrodes after electrodeposition was studied. The absorption increases with increasing cation concentration in the baths, and the highest absorption intensity was obtained for the samples with the highest lead deposit density, which was confirmed by SEM. This work highlights the importance of controlling toxic heavy metal contaminants at low concentrations to improve the performance of CED as an effective method for water treatment and wastewater purification.

ACKNOWLEDGMENTS

The authors gratefully knowledge Qassim University, represented by Deanship of scientific "Research, on the financial support for this research under the number (10130-cos-2020-1-3-I) during the academic year 1442AH/2020AD"

Additional information

Note added by the authors: Ahmed Rebey is the scientific name, but the official name is Hamad AlHadi Rebei. The author is known by the name A. Rebey in Scopus, Google Scholar and ResarchGate.

REFERENCES

[1] T. Thompson, J. Fawell, S. Kunikane, D. Jackson, S. Appleyard, P. Callan, J. Bartram, P. Kingston, S. Water, and World Health Organization, Chemical safety of drinking water: assessing priorities for risk management. World Health Organization, 2007.

[2] L. Wang, Dual-Functional Lead (II) Metal–Organic Framework Based on 5-Aminonicotinic Acid as a Luminescent Sensor for Selective Sensing of Nitroaromatic Compounds and Detecting the Temperature,Journal of Inorganic and Organometallic Polymers and Materials 30 (2019) 291-298.

[3] National Research Council and Safe Drinking Water Committee, An Evaluation of Activated Carbon for Drinking Water Treatment, in: Drinking Water and Health: Volume 2, National Academies Press (US), 1980.

[4] Ehab A. Abdelrahman, R. M. Hegazey, and Ahmed Alharbi,Facile Synthesis of Mordenite Nanoparticles for Efficient Removal of Pb(II) Ions from Aqueous Media,Journal of Inorganic and Organometallic Polymers and Materials 30 (2019) 1369-1383.

[5] N. T. Moja, S. B. Mishra, S. S. Hwang, T. Y. Tsai & A. K. Mishra, Coordination of Lead (II) and Cadmium (II) Ions to Nylon 6/Flax Linum Composite as a Route of Removal of Heavy Metals,Journal of Inorganic and Organometallic Polymers and Materials 6 (2021). DOI:10.1007/S10904-021-02052-8

[6] M. Szklarczyk and J. O. M. Bockris, In situ STM studies of lead electrodeposition on graphite substrate, J. Electrochem. Soc. 137 (1990) 452-457.

[7] W. Zerguine, D. Abdi, F. Habelhames, M. Lakhdari, H. Derbal-Habak, Y. Bonnassieux, D. Tondelier, J. Choi, and J. M. Nunzi, Annealing effect on the optical and photoelectrochemical properties of lead oxide, Eur. Phys. J-Appl. Phys. 84 (2018) 30301.

[8] T. Ishiyama, K. -I. Abe, T. Tanaka, and A. Mizuike, Determination of trace lead in copper by cathodic stripping voltammetry, Anal. Sci. 12 (1996) 263-265.

[9] S. Prakash and V. K. Shahi, Improved sensitive detection of Pb^{2+} and Cd^{2+} in water samples at electrodeposited silver nanonuts on a glassy carbon electrode, Anal. Methods 3 (2011) 2134-2139.

[10] N. Nikolić, P. M. Zivkovic, S. Stevanović, G. Brankovic, Relationship between the kinetic parameters and morphology of electrochemically deposited lead, J. Serb. Chem. Soc. 81 (2016) 553-566.

[11] M. Khelladi, L. Mentar, M. Boubatra, A. Azizi, and A. Kahoul, Early stages of cobalt electrodeposition on FTO and n-type Si substrates in sulfate medium, Mater. Chem. Phys. 122 (2010) 449-453.

[12] Z. Banyamin, P. Kelly, G. West, and J. Boardman, Electrical and optical properties of fluorine doped tin oxide thin films prepared by magnetron sputtering, Coatings 4 (2014) 732-746.

[13] Abhijit Ray, Electrodeposition of Thin Films for Low-cost Solar Cells, Electroplating of Nanostructures, 2015.

[14] J. González-García, J. Iniesta, A. Aldaz, and V. Montiel, Effects of ultrasound on the electrodeposition of lead dioxide on glassy carbon electrodes, New J. Chem. 22 (1998) 343-349.

[15] J. González-García, J. Iniesta, E. Expósito, V. García-García, V. Montiel, and A. Aldaz, Early stages of lead dioxide electrodeposition on rough titanium, Thin Solid Films 352 (1999) 49-56.

[16] J. González-García, F. Gallud, J. Iniesta, V. Montiel, A. Aldaz, and A. Lasia,Kinetics of electrocrystallisation of PbO_2 on glassy carbon electrodes: influence of ultrasound, New J. Chem. 25 (2001) 1195-1198.

[17] J. González-García, F. Gallud, J. Iniesta, M. Montiel, A. Aldaz, and A. Lasia, Kinetics of electrocrystallization of PbO_2 on glassy carbon electrodes. Influence of the electrode rotation, Electroanalysis 13 (2001) 1258-1264.

[18] I. Shtepliuk, M. Vagin, I. G. Ivanov, T. Iakimov, G. R. Yazdi, and R. Yakimova, Lead (Pb) interfacing with epitaxial graphene, Phys. Chem. Chem. Phys. 20 (2018) 17105-17116.

[19] V. Sáez, J. González-García, J. Iniesta, A. Frías-Ferrer, and A. Aldaz, Electrodeposition of PbO_2 on glassy carbon electrodes: influence of ultrasound frequency, Electrochem. commun. 6 (2004) 757-761.

[20] I. Massoudi and A. Rebey, Analysis of in situ thin films epitaxy by reflectance spectroscopy: Effect of growth parameters, Superlattices Microstruct. 131 (2019) 66-85.

[21] O. Oda, Compound semiconductor bulk materials and characterizations, World Scientific, 2007.

[22] W. S. Werner, K. Glantschnig, and C. Ambrosch-Draxl, Optical constants and inelastic electron-scattering data for 17 elemental metals, J. Phys. Chem. Ref. Data 38 (2009) 1013-1092.

[23] H. Yang and R. G. Reddy, Fundamental studies on electrochemical deposition of lead from lead oxide in 2: 1 urea/choline chloride ionic liquid, J. Electrochem. Soc. 161 (2014) D586.

[24] N. Sugumaran, P. Everill, S. W. Swogger, and D. P. Dubey, Lead acid battery performance and cycle life increased through addition of discrete carbon nanotubes to both electrodes, J. Power Sources 279 (2015) 281-293.

[25] N. D. Nikolić, V. M. Maksimović and G. Branković, Morphological and crystallographic characteristics of electrodeposited lead from a concentrated electrolyte, RSC Adv. 3 (2013) 7466-7471.

[26] C. -Z. Yao, M. Liu, P. Zhang, X. -H. He, G. -R. Li, W. -X. Zhao, P. Liu, and Y. -X. Tong, Tuning the architectures of lead deposits on metal substrates by electrodeposition, Electrochim. Acta 54 (2008) 247-253.

[27] J. Matthews, Accommodation of misfit across the interface between single-crystal films of various face-centred cubic metals, Philos. Mag. 13 (1966) 1207-1221.

[28] G. Arrhenius, X-ray diffraction procedures for polycrystalline and amorphous materials, ACS Publications 228 (1955).

[29] S. S. Djokić, Electrodeposition and Surface Finishing. Springer: New York, NY, USA (2014).

[30] K. I. Popov, E. R. Stojilković, V. Radmilović, and M. G. Pavlović, Morphology of lead dendrites electrodeposited by square-wave pulsating overpotential, Powder Technol. 93 (1997) 55-61.

[31] N. D. Nikolić, K. I. Popov, E.R. Ivanović, G. Branković, S. I. Stevanović, and P. M. Živković, Thepotentiostatic current transients and the role of local diffusion fields in formation of the 2D lead dendrites from the concentrated electrolyte, J. Electroanal. Chem. 739 (2015) 137-148.

[32] S. Cherevko, X. Xing, and C. H. Chung, Hydrogen template assisted electrodeposition of sub-micrometer wires composing honeycomb-like porous Pb films, Appl. Surf. Sci. 257 (2011) 8054-8061.

[33] N. D. Nikolic, K. I. Popov, P. M. Zivkovic, and G. Brankovic, A new insight into the mechanism of lead electrodeposition: Ohmic-diffusion control of the electrodeposition process, J. Electroanal. Chem. 691 (2013) 66-76.

[34] A. Rajamani, U. B. R. Ragula, N. Kothurkar, and M. Rangarajan, Nano-and micro-hexagons of bismuth on polycrystalline copper: electrodeposition and heavy metal sensing, CrystEngComm. 16 (2014) 2032-2038.

[35] S. Gupta, R. Singh, M. Anoop, V. Kulshrestha, D. N. Srivastava, K. Ray, S. Kothari, K. Awasthi, and M. Kumar, Electrochemical sensor for detection of mercury (II) ions in water using nanostructured bismuth hexagons, Appl. Phys. A 124 (2018) 737.

[36] A. Zimmer, L. Broch, C. Boulanger, and N. Stein,Morphological and chemical dynamics upon electrochemical cyclic sodiation of electrochromic tungsten oxide coatings extracted by in situ ellipsometry, Electrochim. Acta 174 (2015) 376-383.

[37] M. Paunovic and M. Schlesinger, Fundamentals of electrochemical deposition, John Wiley & Sons, Inc., Hoboken, New Jersey, 2005.

[38] Y. Katayama, R. Fukui, and T. Miura, Electrodeposition of lead from 1-butyl-1-methylpyrrolidinium Bis(trifluoromethylsulfonyl)amide ionic liquid. J. Electrochem. Soc. 160 (2013) D251-D255.

[39] A. Liu, Z. Shi, and R.G. Reddy, Electrodeposition of Pb from PbO in urea and 1-butyl-3-methylimidazolium chloride deep eutectic solutions. Electrochim. Acta 251 (2017) 176-186.

Dear Editors,

No conflict of interest exists in the submission of this manuscript, and the manuscript is approved for publication. Also, I would like to declare that the described work is original research.

Sincerely yours,

Corresponding author,